Solar Energy 204 (2020) 337–345

Contents lists available at ScienceDirect

Solar Energy

journal homepage: www.elsevier.com/locate/solener

Thermal assisted blade coating methylammonium lead iodide films with non-toxic solvent precursors for efficient perovskite solar cells and sub-module

Kun-Mu Lee[a,b,c,d,*], Chia-Hsin Lai[a], Wei-Cheng Chu[a], Shun-Hsiang Chan[a,c], Vembu Suryanarayanan[e]

[a] Department of Chemical and Materials Engineering, Chang Gung University, Taoyuan 33302, Taiwan
[b] Division of Neonatology, Department of Pediatrics, Chang Gung Memorial Hospital, Linkou, Taoyuan 33305, Taiwan
[c] Green Technology Research Center, Chang Gung University, Taoyuan 33302, Taiwan
[d] Center for Reliability Sciences and Technologies, Chang Gung University, Taoyuan 33302, Taiwan
[e] Electroorganic Division, CSIR-Central Electrochemical Research Institute, Karaikudi 630003, India

ARTICLE INFO

Keywords:
Perovskite solar cell
Thermal assisted blade coating
Large area
Sub-module
Non-toxic solvents

ABSTRACT

Atmospheric thermal assisted blade coating (TABC) method, which is quick film crystallization and easier fabrication than the commonly used spin-coating process, to prepare a high quality $CH_3NH_3PbI_3$ perovskite film is investigated in this work. Selection of the perovskite precursor solvents and controlling the ratio of the mixed solvent as well as substrate temperature for perovskite film formation are important factors in this TABC process. Based on the results obtained in this work, substrate temperature is the key factor for managing the perovskite film phase transition which influences the film roughness and crystallinity. Furthermore, the high-quality perovskite films are prepared by perovskite precursors with mixture of solvents containing GBL/DMSO at the ratio from 1/9 to 5/5. By using the optimum substrate temperature of 130 °C and the GBL/DMSO solvent ratio of 1/9 (G01D09) for the preparation of small area n-i-p and p-i-n PSCs as well as the p-i-n type perovskite sub-module, the power conversion efficiencies of 17.55%, 16.90% and 13.03%, respectively, are acquired under the illumination of 100 mW/cm^2 (AM 1.5G).

1. Introduction

Since the first appearance in 2009, organic-inorganic hybrid perovskite solar cells (PSCs) have performed promising future due to their relative low cost and the skyrocketed power conversion efficiency (PCE) in a short period. The rapid improvement of the PCE from 3.9% (Kojima et al., 2009) to more than 25% (Laboratory, 2018) shows the potential of the commercialization of the perovskite solar cells. Owing to the advantages of perovskite such as excellent light harvesting, high carrier mobility, good carrier diffusion length and lifetime (Leijtens et al., 2016; Wetzelaer et al., 2015), various technologies are being developed for depositing high quality perovskite films with large grains and solar cell devices with superior photoelectric properties. The spin-coating is a most widely used technique to fabricate high-quality perovskite films because of the simple procedure. The perovskite film quality is controlled by the process conditions like spinning speed, precursor solution concentration and annealing temperature. However, this method is only suitable for lab-scale cells, where the films are not uniform from center to edge during device up-scaling. Furthermore, the process cost will increase because of the involvement of waste raw materials and solvents during spin-coating process, and use of toxic solvents such as N,N-dimethylformamide (DMF), toluene and chlorobenzene as well as additives required in further steps to improve the crystallization, film uniformity and reducing chemical defects (Lee et al., 2019; Paek et al., 2017; Tavakoli et al., 2019; Xu et al., 2019). Finding alternatives to spin coating and hazardous solvents that meet the stringent requirements demanded by large scale production is of high priority.

According to the challenges of scalable film deposition with uniformity and repeatability, several film deposition processes have been applied to large-scale perovskite solar cell production, such as blade coating (Bi et al., 2018; Deng et al., 2015a; Kim et al., 2015; Tang et al., 2020), spray coating(Barrows et al., 2014; Das et al., 2015), slot-die coating(Cotella et al., 2017; Qin et al., 2017; Whitaker et al., 2018),

* Corresponding author at: Department of Chemical and Materials Engineering, Chang Gung University, Taoyuan 33302, Taiwan.
E-mail address: kmlee@cgu.edu.tw (K.-M. Lee).

https://doi.org/10.1016/j.solener.2020.05.003
Received 22 March 2020; Received in revised form 22 April 2020; Accepted 3 May 2020

inkjet printing(Li et al., 2015; Wei et al., 2014), dip coating(Liang et al., 1998), and electrodeposition process(Chen et al., 2015). Among the methods mentioned above, blade coating is the most appealing process with simple instrument, easy-made, effective material use, low-cost and no coating limitation. Also, the possibility of integration into slot-die coating process is considered feasible. Besides, blade coating is a process where the film thickness and smoothness can be easily controlled by the speed of blade, the gap between blade as well as substrate, the temperature of the substrate and the concentration of the precursor. Perovskite films prepared by blade coating have been developed in several ways, including fabrication in ambient air (Yang et al., 2015), combining air flow-assisted PbI_2 (Razza et al., 2015) and anti-solvent extraction method (Yang et al., 2017). Studies of the nucleation as well as crystallization behaviors of perovskite film (Deng et al., 2015b; Ye et al., 2017) had been well documented. Huang et al. have investigated the fabrication of blade-coated perovskite layers and devices by tuning the perovskite composition and their blade-coated films having unique domain structure with lateral sizes varying from 80 to 250 μm under various processing temperatures (Deng et al., 2015a). They used heated substrates during blade coating and correctly argued that the creation of cellular convective motion or Benard cells is responsible for the formation of large perovskite domains, which results in a longer carrier diffusion length and reduced charge recombination, thus improving the device performance(Deng et al., 2016). The thermal assisted blade coating (TABC) could get large perovskite domains and high film coverage without using anti-solvent which is similar to the hot-casting spin coating process. Such perovskite film obtained by TABC process can get a large area film with uniform thickness which is better than hot-casting spin coating process.

Moreover, the fabrication of lead halide perovskites with non-toxic solvents by industrially relevant techniques is very important and needs improvement. In this study, we use dimethyl sulfoxide (DMSO) and γ-butyrolactone (GBL) as mixed solvent for high concentration perovskite precursor solutions and analyzed the effect of solvent on cohesion or expansion behaviors of the perovskite films. The effects of substrate temperature and mixed solvent ratio of the precursor solution on the formation of perovskite film by TABC process are also investigated. The crystallization of perovskite film, crystal growth orientation, surface morphology, and film coverage for high efficiency and stable PSCs are systematically explored. It is found that the perovskite films become very rough if precursor solvent used is DMSO or GBL. Further, a controlled substrate temperature of 130 °C with the precursor GBL/DMSO solvent ratio of 1/9 leads to the best quality of $CH_3NH_3PbI_3$ film and PSC photovoltaic performance. It is also noted that the precursor concentrations for the best PCE of n-i-p PSC and p-i-n PSC are different by this TABC process. Finally, the efficiencies of more than 17% and 13% of small cell PSC and PSC sub-module, respectively, are observed.

2. Experimental

2.1. Material preparation

CH_3NH_3I (MAI) was synthesized by reacting 50 ml CH_3NH_2 (33 wt% in absolute ethanol, Aldrich) and 20 ml HI (57 wt% in water, Aldrich) in a 250 ml round-bottom flask at 0 °C for 2 h with stirring. The precipitate was recovered by evaporation at 55 °C for 1 h. The MAI was then dissolved in ethanol, recrystallized from diethyl ether, and dried at 60 °C in a vacuum oven for 24 h. The perovskite precursor solution was prepared by mixing PbI_2 (99.9 wt%, Aldrich) and CH_3NH_3I at molar ratio of 1:1 in the co-solvent system of dimethylsulfoxide (DMSO): γ-butyrolactone (GBL) with a total concentration of 40 wt%.

3. PSC device fabrication

FTO glass (7 Ω/square) was cleaned by sonication sequentially with neutral wash solution (Extran® MA 02, Merck Inc.), acetone, and isopropyl alcohol for 10 min, respectively. After drying the substrate, PEDOT:PSS (HeraeusClevios™ P VP AI 4083) film was spin coated onto the clean substrate at 5000 rpm for 50 s from its aqueous solution filtered with a 0.45 mm filter, and then thermal annealed at 125 °C for 30 min in the air. The perovskite precursor solution (40 wt%, the volume ratio of solvents were GBL/DMSO = 0/10, 1/9, 3/7, 5/5, 7/3, 9/1 and 10/0, which were named as G00D10, G01D09, G03D07, G05D05, G07D03, G09D01 and G10D00, respectively) was dropped onto preheated PEDOT:PSS-covered FTO substrate on a hot plate with controlled temperatures from 70 to 150 °C, and then was blade coated onto the substrate at a speed of 2 cm/s with blade gap of 300 μm by a small coating machine with metal blade (ZEHNTNER, ZUA 2000). The amount of perovskite precursor solution on a 2 cm × 5 cm substrate was 30 μL for TABC method, and the amount of precursor solution on a 2 cm × 2 cm substrate was 80 μL for spinning coating method. The amount of perovskite precursor for TABC was indeed less than that for spin coating method.

The resulting films were annealed at 130 °C for 1 min after blade coating step (Two hot plates (P1 and P2) were used for this TABC process. One hot plate (P1) was controlled at the various coating temperatures; another one (P2) was set at 130 °C. We coated the perovskite films on P1 and quickly moved the substrate to P2 for 1 min after finishing the coating process on P1). These layers were fabricated under ambient air and humidity (30–40%). Finally, C60 (50 nm), BCP (5 nm), and Ag electrode (100 nm) were deposited by thermal evaporation sequentially, and the active area of this electrode was fixed at 0.16 cm^2 for small cell PSC and 10.56 cm^2 for PSC sub-module.

The fabrication of n-i-p PSC involves the deposition of TiO_2 compact blocking TiO_x layer onto the FTO glass by spray pyrolysis by a solution of titanium diisopropoxidebis(acetylacetonate) (75 wt% of Ti $(acac)_2OiPr_2$ in isopropanol) at 450 °C and the fabrication of the mesoporous TiO_2 layer (150 nm, particle size 20 nm, anatase) was done by screen printing with home-made TiO_2 pastes followed by annealing to 500 °C for 30 min. The perovskite film was deposited by aforementioned blade coating method and fabricated under ambient air and humidity (30–40%). The hole-transporting material (HTM) solution involving Spiro-OMeTAD (50 mg/mL), 17.5 μL of a solution of lithium bis(trifluoromethane)sulfonamide (Li-TFSI) in acetonitrile (520 mg/mL) and 28.5 μL 4-*tert*-butylpyridine (TBP) was added into chlorobenzene simultaneously. The HTM was spin-coated onto the $CH_3NH_3PbI_3$ film at 2000 rpm for 30 s. Finally, Ag electrode (100 nm) was deposited by thermal evaporation, and the active area of Ag electrode was fixed at 0.16 cm^2.

4. Solar cell performance measurement

Conversion efficiencies of PSCs were evaluated under simulated one sun irradiation from a Xe arc lamp with an AM 1.5 global filter (SS-F5-3A, ENLI Technology Co. Ltd., Taiwan). Irradiance was characterized using a calibrated spectrometer and illumination intensity was set using an NREL certified silicon diode with an integrated KG5 optical filter: spectral mismatch factors were calculated for each device in this report to be less than 5%. J-V curves were recorded with a Keithley 2400 source meter under the simulated AM 1.5G sunlight, calibrated to 100 mW/cm^2. The reported device characteristics were estimated from the measured J-V curves. IPCE spectra were measured in air using a commercial IPCE set-up (QE-R, ENLI Technology Co. Ltd., Taiwan).

5. Results and discussion

5.1. Effect of substrate temperature

In this section, the substrate temperature ranging from 70 to 150 °C on the film formation is studied (Because of at too low temperature, the film after coating is still wet; at too high temperature, the solvent evaporates too quickly to complete the coating process). Fig. 1 reports

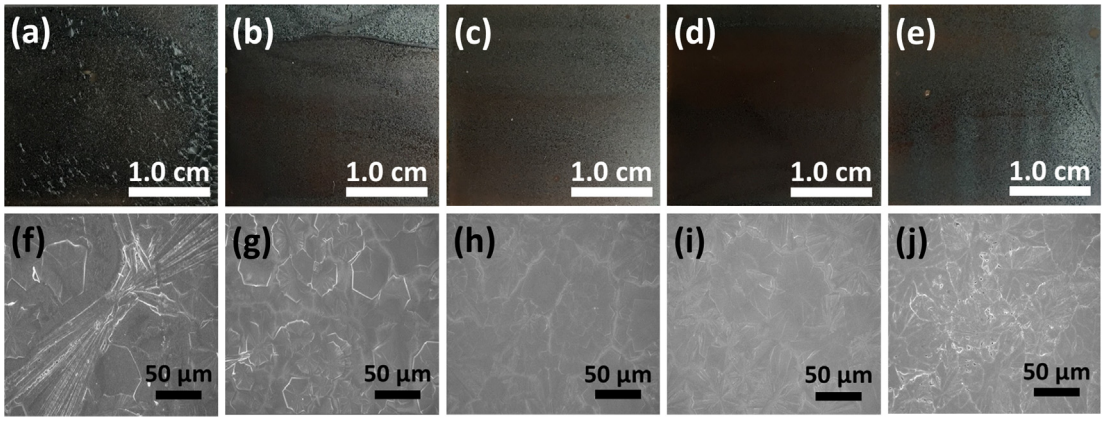

Fig. 1. Optical microscopy (OM) ((a) to (e)) and SEM ((f) to (j)) Images of thermal assisted blade coated $CH_3NH_3PbI_3$ perovskite films at various substrate temperatures. (a), (f) 70 °C; (b), (g) 90 °C; (c), (h) 110 °C; (d), (i) 130 °C, and (e), (j) 150 °C.

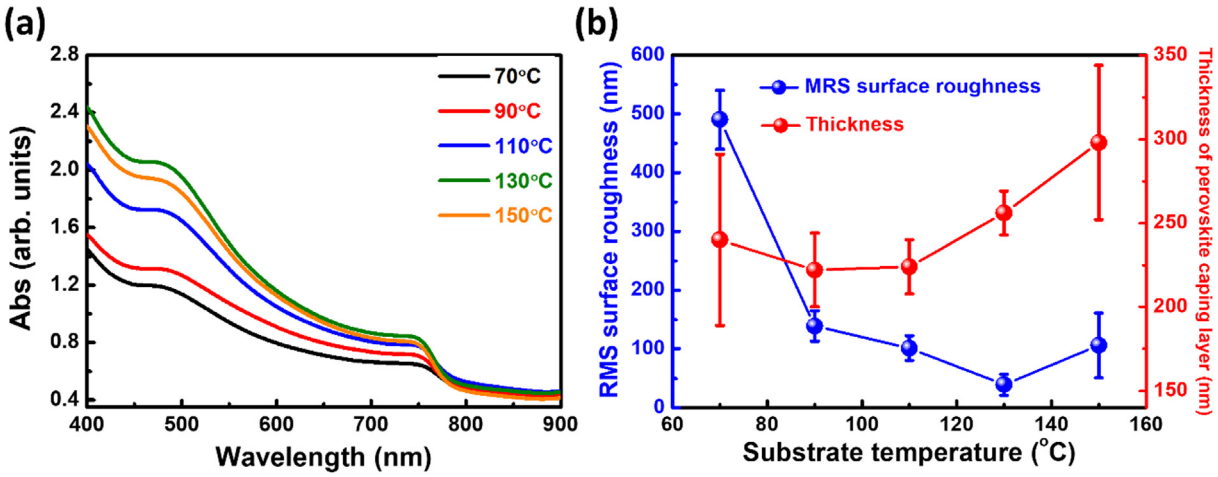

Fig. 2. (a) UV–vis spectra and (b) thickness and RMS surface roughness of TABC $CH_3NH_3PbI_3$ perovskite films prepared at various substrate temperatures.

the optical microscopy (OM) and SEM images of perovskite films prepared under various temperatures. The perovskite films prepared at 70 °C show perovskite aggregates of uneven film which is due to precursor solution flowing on the substrate causing variable evaporation rates of solvents. The film quality gradually improved as the substrate temperature was increased. It is also found that perovskite film prepared at 110 and 130 °C shows larger domain size and smoother films, and that at 150 °C shows uneven perovskite film again due to the formation of discontinuous particles or pinholes in some areas. Fig. 2 shows (a) UV–vis spectra and (b) thickness and RMS surface roughness of TABC $CH_3NH_3PbI_3$ perovskite films prepared at various temperatures. The typical UV–vis absorption spectrum of $CH_3NH_3PbI_3$ perovskite film starting from wavelength of 770 nm has another shoulder at 500 nm. The difference of UV–vis absorption intensities between various temperatures are from film thickness (Increase of temperature leads to the thicker film). The RMS roughness of film prepared at 130 °C has the value of 39.43 nm, which is the lowest RMS roughness of all prepared conditions, and this can also correspond to the SEM image results.

The crystalline properties of the $CH_3NH_3PbI_3$ films on *meso*-TiO_2 film and PEDOT:PSS film with various temperatures were further evaluated by XRD diffraction patterns (Fig. 3). It is interested to note that $CH_3NH_3PbI_3$ perovskite films show differences in the crystallite orientation with respect to the substrates. The perovskite films fabricated on *meso*-TiO_2 film are oriented over 110 plane at 70 and 90 °C and over 112 plane at 110 and 130 °C; however, those fabricated on PEODT:PSS are preferentially oriented over 112 plane on the substrate during 70–130 °C. The films are over 110 and 112 planes together when prepared at high temperature of 150 °C on both substrates. Moreover, the peak intensities corresponding to 112 plane are much higher than those of 110 plane which reflects the highly crystalline nature of the prepared perovskite films. The crystal size trend of coating at each temperature is that the higher the temperature is, the larger will be the grain size (before 130 °C), and has the largest size of 64.5 nm for that film prepared at 130 °C.

Fig. 4 exhibits the PL spectral and TRPL analysis. This analysis shows the carrier collection and transport properties in PSC. Fig. 4(a) shows that perovskite films prepared at low temperature (70–90 °C) have the strongest photoluminescence intensity, which may be contributed by the presence of many traps in perovskite films. In contrast, for perovskite films prepared at higher temperatures (110–150 °C), less defects in the films results in in less recombination and lower PL intensity. Fig. 4(b) shows the obvious difference in carrier lifetime and the detailed fitting data is listed in Table S1. The lower the coating temperature is, the poorer will be the perovskite film-formation and crystallinity, as well as the longer the carrier transfer time (τ_1) and recombination time (τ_2). Perovskite film prepared at 130 °C has the shortest life time (4.47 ns).

In terms of photovoltaic performance, the J-V curves of p-i-n PSC with perovskites prepared at various temperatures are revealed in Fig. 5 and photovoltaic characteristics are listed in Table 1. The statistical efficiency distribution of the cells is arranged in Fig. S1. The highest efficiency of PSC coated at 70 °C can reach about 8.35%, but the efficiency distribution is large (from 1% to 8%). This is due to the fact that

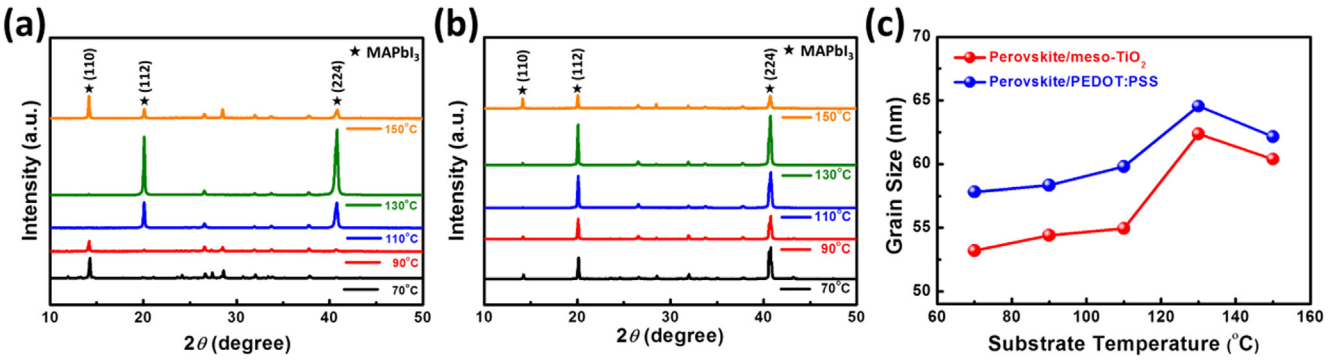

Fig. 3. XRD analysis of blade coated $CH_3NH_3PbI_3$ perovskite films at various substrate temperatures. (a) PVSK/*meso*-TiO_2/FTO glass, (b) PVSK/PEDOT:PSS/FTO glass, and (c) grain sizes of perovskite films on substrates.

the solvent evaporation rate of perovskite precursor is slow at lower temperature after coating, and it produces few addition compounds such as MAI·PbI_2·DMSO, PbI_2·DMSO and PbI_2 with needle-like crystals, resulting in poor film coverage. On the other hand, although there is no complex formation at high temperature blade coating, the cell efficiency of PSC with perovskite film prepared at 150 °C reached to 15.91%. The fast solvent evaporation rate and difficulty in the control of manual blade coating result in clumping or incomplete coverage of few parts of the perovskite film. Those devices with such films show poor efficiencies. The efficiency distribution of PSCs with perovskite prepared at 130 °C have the narrowest distribution, which are between 14% and 17% efficiency, due to the direct nucleation of precursor solution. This grows into large-sized perovskite grains during TABC process, in which it completely covers and forms a dense flat film. This can be proved from the film surface analysis as well as device performance. This reveals that the coating parameters and the film crystallization control have the best match under this condition, which is better than that of fabricated one by spin coating process (as shown in Fig. S1). The TABC process involving the growth of $CH_3NH_3PbI_3$ films have the desired perovskite structure and this can be obtained after short-term thermal annealing process, because the precursor solution and the substrate can be *in-situ* heated to the temperature that favors $CH_3NH_3PbI_3$ formation. These results can also be used as a basis for coating on a larger area and a uniform perovskite film for PSC submodule.

5.2. GBL/DMSO solvent ratio effect

It is known that the solvent of the precursor solution significantly affects the state and quality of perovskite film formation, which influences the performance of the PSC. The DMF, commonly used in the literatures, is highly toxic in nature, while GBL as well as DMSO are comparatively less toxic than the former and have good solubility. Some literatures have explored the film formation mechanism of precursors with GBL and DMSO (Jung et al., 2019; Liu et al., 2018; Xie et al., 2017). The thermal convection of precursor solution is the key to this procedure. While GBL is used as a solvent for the perovskite precursor, the thermal convection flow direction of GBL during heating is from the center to the periphery. Therefore, the perovskite aggregates form a ring-like morphology, which makes the film uneven and poorly covered. When DMSO is used as the solvent, the thermal convection direction is from the periphery to the center, leading to the formation of a bump-like surface and this also makes the film uneven and poorly covered.

It is observed that the boiling point of GBL is 204 °C, which is higher than that of DMSO (189 °C). Similarly, the surface tension (at 25 °C) of DMSO (43.6 mN/m) is greater than that of GBL (35.4 mN/m). With the use of GBL/DMSO mixed solvents, the difference in surface tension can generate a driving force that causes the solvents to pass from the periphery to the center, resulting in an inverted convection. The balance of convection and inverted convection can deposit a platform-like morphology, which makes the perovskite film flat and has a good coverage. Therefore, we systematically designed several solvent ratios of GBL/DMSO (v/v), which are 0/10, 1/9, 3/7, 5/5, 7/3, 9/1 and 10/0, represented by the following symbols such as G00D10, G01D09, G03D07, G05D5, G07D03, G09D01 and G10D00, respectively.

The SEM and AFM images of perovskite films prepared by various GBL/DMSO solvent ratios are reported in Fig. 6. It is found that the crystal of G00D10 is a sheet-like structure that diverges outward from the center. Wherever, the proportion of DMSO in the solvent decreases,

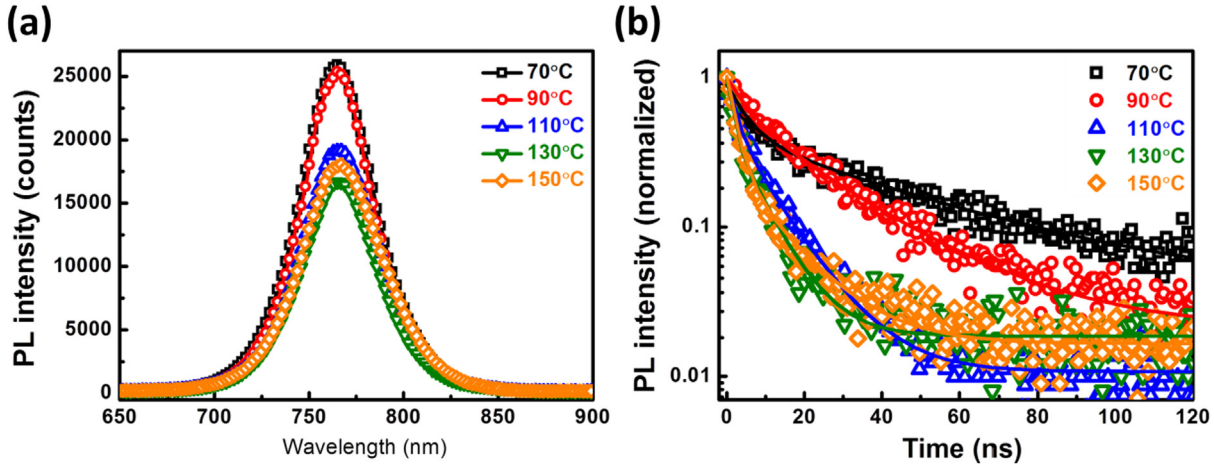

Fig. 4. (a) PL and (b) TRPL behavior of blade coated perovskite films on PEDOT:PSS/FTO glass at various substrate temperatures.

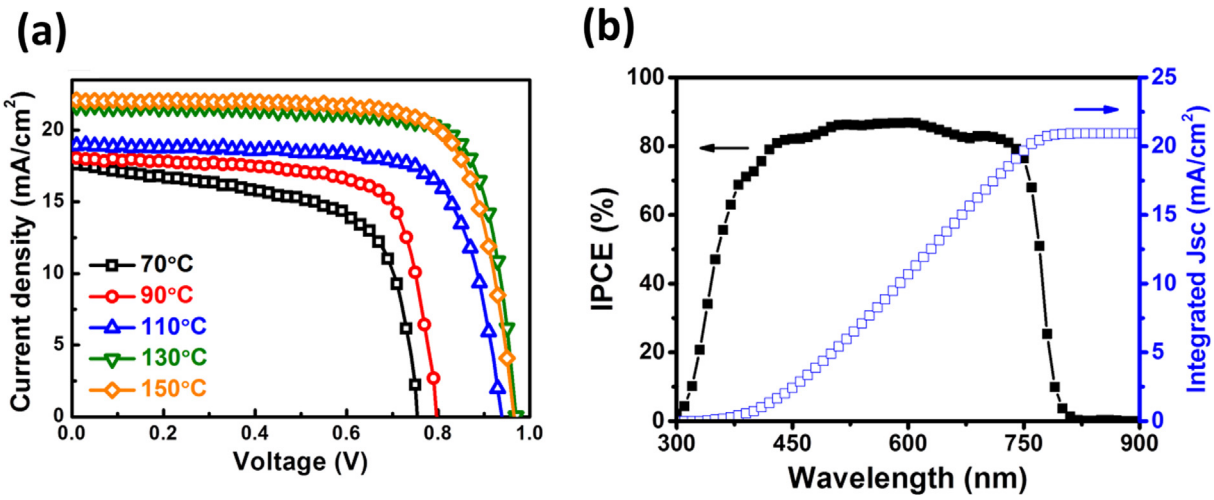

Fig. 5. (a) J-V curves of p-i-n PSCs with TABC perovskite films at various substrate temperatures. (b) The IPCE spectra and integrated J_{SC} of PSC prepared at 130 °C.

Table 1
Photovoltaic characteristic of p-i-n PSCs with blade coated perovskite films at various substrate temperatures.

Substrate temp. (°C)	J_{SC} (mA/cm^2)	V_{OC} (V)	FF	PCE (%)
70	17.38	0.755	0.636	8.35
90	17.96	0.796	0.729	10.42
110	18.90	0.939	0.730	12.96
130	21.71	0.970	0.762	16.05
150	22.05	0.966	0.747	15.91

the more will be the nucleation points leading to smaller crystal size. If the proportion of DMSO in the solvent, such as G00D10 and G01D09 is large, the crystal structure will be more complete. For example, in G07D03, the small crystal structure leads to more boundaries. When the proportion of DMSO is very small, (for example in G09D01 and G10D00), the surface of the film is extremely rough (the RMS roughness of films are shown in Fig. 7(b)). The uneven film affects the coverage of the subsequent coating of electron or hole transport layers. Therefore, it is better to choose the precursor with higher proportion of DMSO when preparing the perovskite film by TABC process.

Fig. 7(a) shows the qualitative XRD analysis of $CH_3NH_3PbI_3$ perovskite film. The grain size and signal strength of the main crystal phases of perovskite with the 2Θ values of 20.1° (1 1 2) and 40.2° (2 2 4) vary with the ratios of DMSO in the precursor solution, and the grain size increases with the DMSO ratio and up to ~54 nm under G01D09 condition (Fig. 7(b)). From the full width half maximum (FWHM) of PL mapping (Fig. 7(c)), we see that the relatively flat perovskite films (G01D09 to G05D05) have similar PL FWHM over the mapping region (1000 μm × 1000 μm) and perovskite films prepared from single solvent (G10D00 and G00D10) exhibit a higher and wide distribution of FWHM. In addition, we also confirm that the PL intensity decreases as the ratio of DMSO in precursor solution increases and the G01D09 has the best behavior, which is shown in Fig. S2. This indicates that a larger grain size and a flat perovskite film can achieve a lower film defect density.

The power conversion efficiencies (PCEs) of p-i-n PSCs and n-i-p PSCs prepared with various ratios of GBL/DMSO precursors are reported in Fig. 8. The two types of PSCs show the same trend of CPEs which may be improved with the increase of DMSO ratio, and the best condition is G01D09. The PSCs prepared by single solvent (G00D10 and G10D00) show lower J_{SC} which is due to the rough film surface with a thin film. This can be demonstrated by the above description of single solvent film formation. Furthermore, we also explore the effect of different precursor solution concentrations. It is interesting to note that the optimal concentration for p-i-n PSC is 1.25 M, while for n-i-p PSC, it is 1.65 M. The reason may be due to the fact that various surface forces between the precursor solution and different substrates (PEDOT: PSS and TiO_2) affect the film formation and the optimal precursor solution concentration. This phenomenon can also be echoed with the XRD

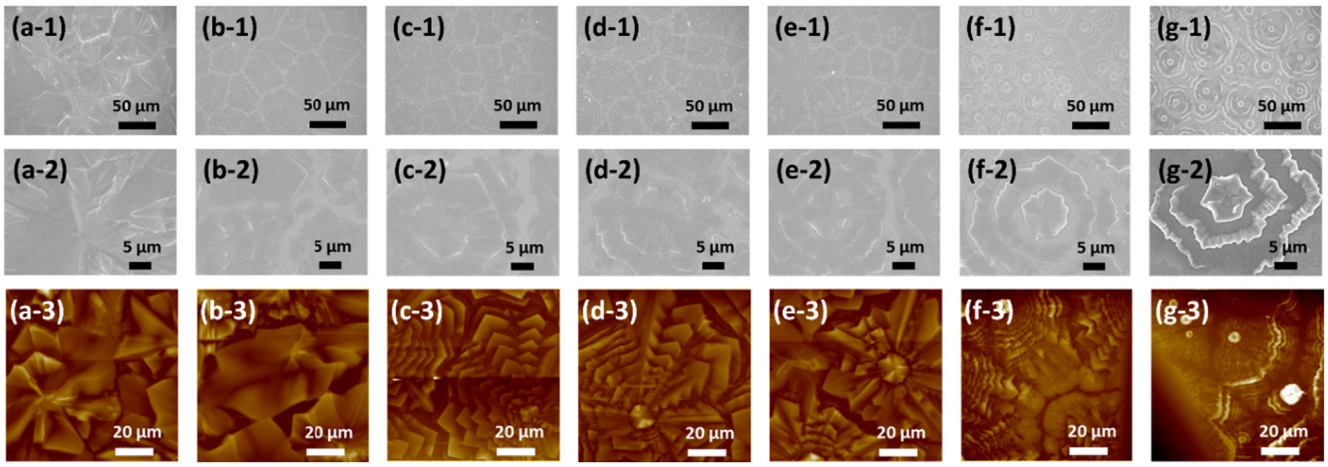

Fig. 6. SEM and AFM images of TABC $CH_3NH_3PbI_3$ perovskite films with various GBL/DMSO solvent ratios. (a) G00D10, (b) G01D09, (c) G03D07, (d) G05D05, (e) G07D03, (f) G09D01, and (g) G10D00.

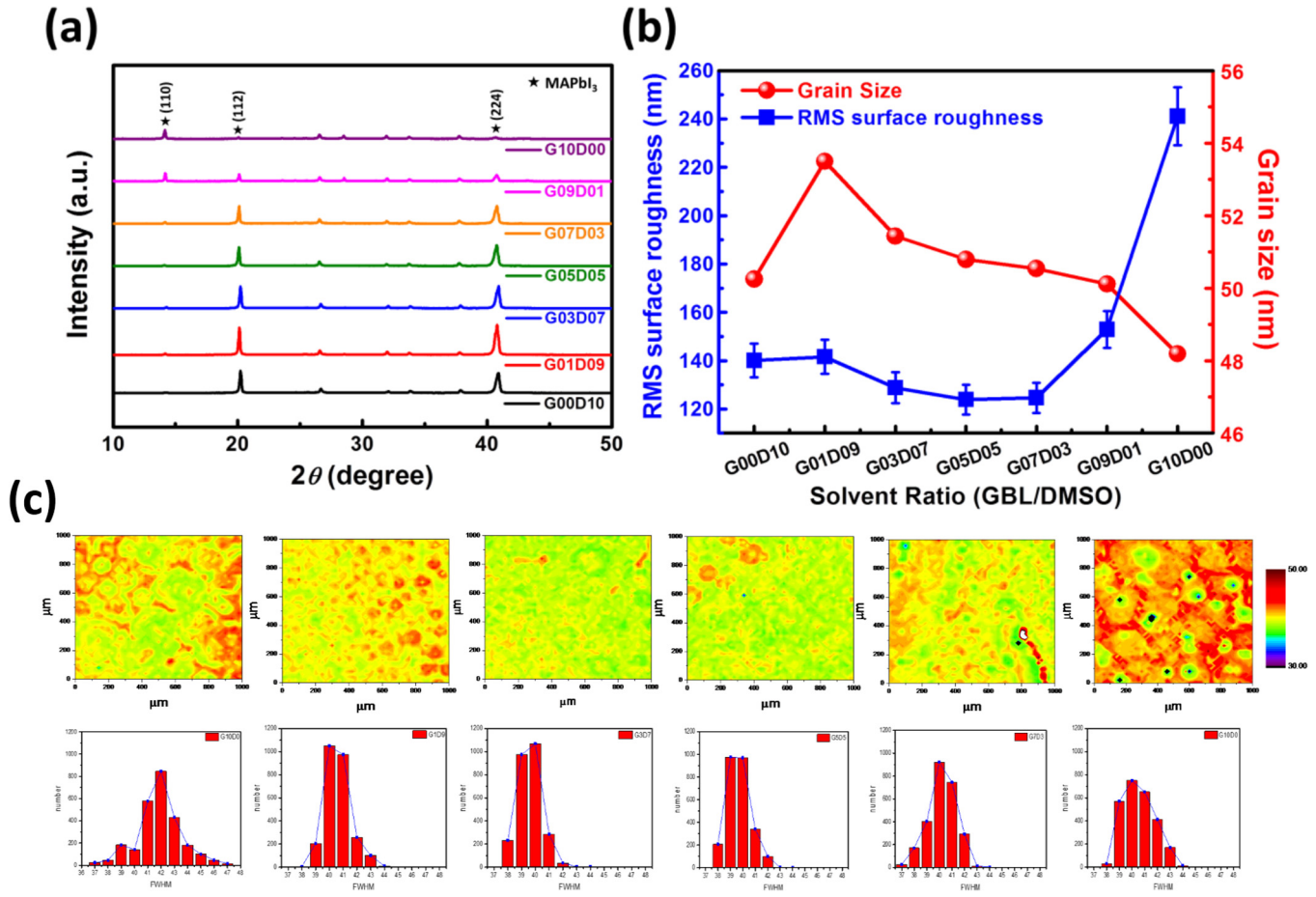

Fig. 7. (a) XRD analysis and grain size, (b) RMS surface roughness and (c) FWHM of PL mapping (1000 μm × 1000 μm) of TABC perovskite films with various GBL/DMSO solvent ratios.

analysis in Fig. 3 taken under different substrate materials and temperature conditions, where the perovskite film crystal plane phase direction and film quality are indeed affected. Fig. 9 shows the best performance of p-i-n and n-i-p PSCs. There is almost no hysteresis in the forward and reverse sweep in J-V curves of p-i-n PSC and has the best PCE of 16.9%; while the J-V curves of n-i-p PSC show a slight J-V curves hysteresis behavior, but has the higher PCE of 17.55%. Moreover, we can see from the efficiency statistics chart that the TABC process is suitable for a large area preparation and there is no obvious regional difference, where the efficiency of the PSC has a centralized distribution. In comparison, the perovskite film prepared by spin coating process is susceptible to some conditions such as rotary centrifugal force and anti-solvent drop (solvent amount, drip time and etc.). The properties of the center and periphery of the perovskite film prepared on substrate are likely to be different. Optimal perovskite often appears only in the center area of the film and relatively high roughness of the peripheral film. Therefore, although the maximum efficiency of PSC prepared by the spin coating process is 17–18%, the statistical efficiency of PSCs is widely distributed. This means that the spin coating process is not suitable for fabricating large-area PSCs.

Finally, we explore the efficiency of PSCs with various active areas (Fig. 10(a)) and the effectiveness of PSC sub-module (Fig. 10 (b) to (d)). PSC with an active area of 4 mm × 4 mm (0.16 cm^2) has the highest efficiency, and the PCE has no significant drop as the active areas are enlarged to 5 mm × 5 mm or even 7 mm × 7 mm.The active area is further enlarged to 11 mm × 11 mm (1.21 cm^2), and the PSC efficiency still have an excellent performance of > 15%, which proves the quality of the highly uniform perovskite film made by TABC process. Based on the good results of small cell PSC, we demonstrate a sub-module PSC that constructed from a series connection of six cells (substrate area: 25 cm^2 and active area: 10.56 cm^2). The schematic, photograph and J-V curve of the sub-module PSC are shown in Fig. 10(b)–(d). The CO_2-laser patterned FTO was adopted to fabricate an integrated series connection between the cells in the sub-module. The J_{SC}, V_{OC}, FF and PCE of 3.52 mA/cm^2, 5.41 V, 0.684 and 13.03%, respectively, were achieved under 1 sun illumination. The current and voltage performance of the PSC sub-module are similar to those of the small cell PSC, which means the well control and uniformity of perovskite as well as other layers in this PSC sub-module, however the PCE shows slightly lower which is mainly due to the lower FF value. This can be solved by improving the series resistance between the cells inside the module in the future.

6. Conclusions

In this study, the high quality $CH_3NH_3PbI_3$ perovskite film was prepared by the TABC process. We found that there is a greater chance to get the uniform and excellent crystalline films when coating temperature is in the range of 110–150 °C and the optimal process temperature is at 130 °C. In addition, the perovskite film formation is affected obviously by the ratio of GBL/DMSO in precursor solution, where G01D09 shows the best condition. Film quality and PSCs efficiency can be mutually verified although the precursor concentrations for the best PCE of n-i-p PSC and p-i-n PSC are different. The efficiencies of 17.55% and 13.03% of small cell PSC and PSC sub-module respectively were obtained. The excellent performance in each type PSCs (small cell and sub-module) illustrates the advantages of the TABC process for fabricating large-area PSCs.

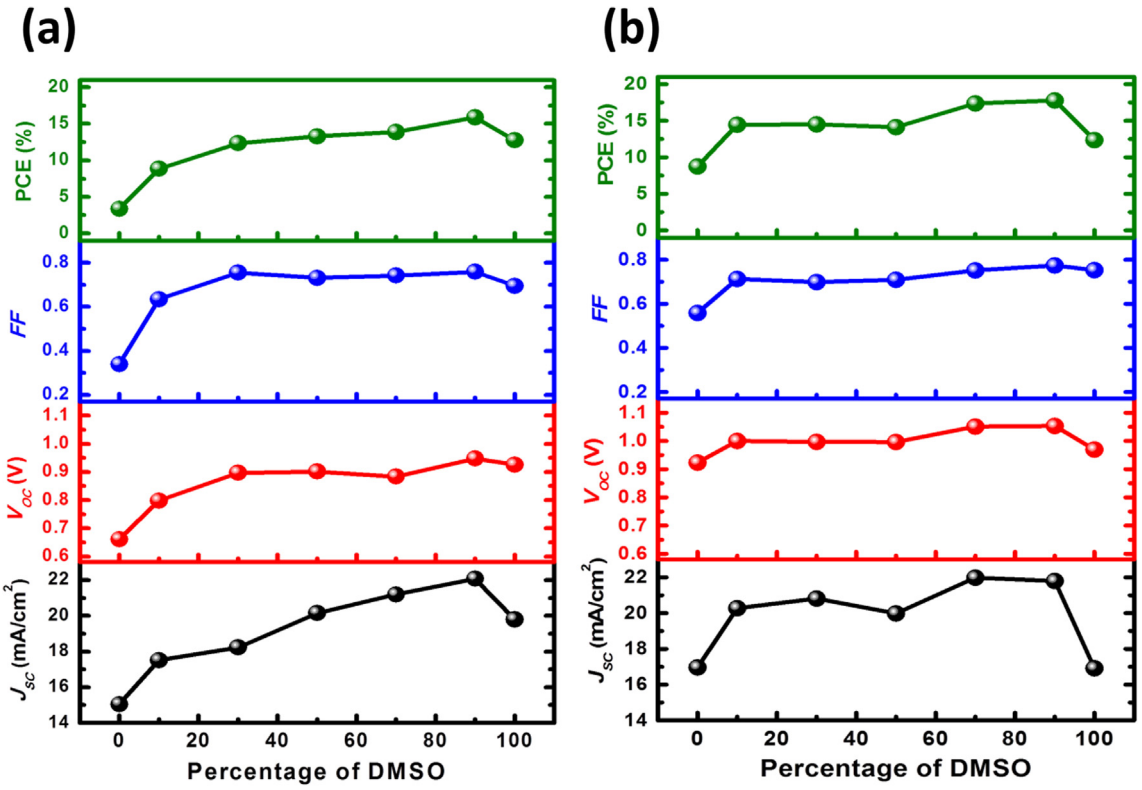

Fig. 8. Photovoltaic characteristic of PSCs with TABC perovskite films of various GBL/DMSO solvent ratios. (a) p-i-n PSC and (b) n-i-p PSC.

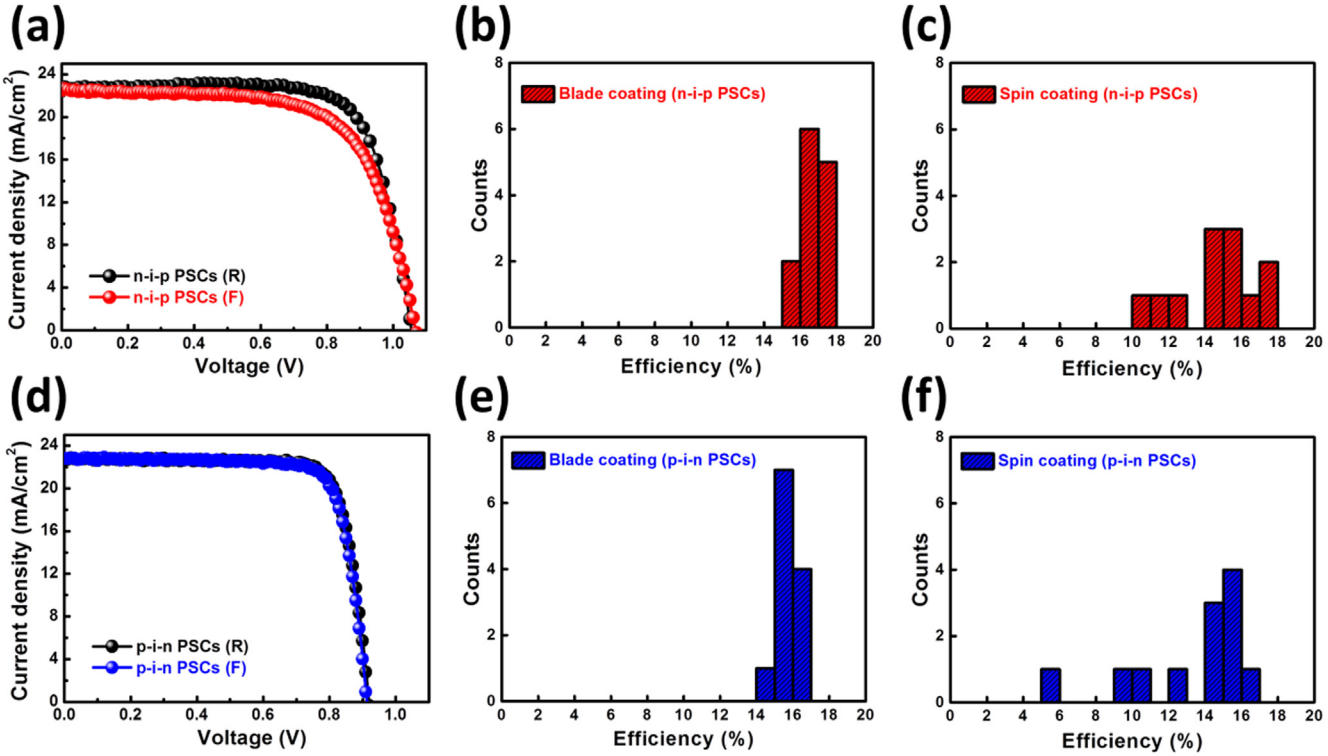

Fig. 9. Best J-V performance of (a) n-i-p PSC and (d) p-i-n PSC by TABC process, and efficiency distribution of PSCs (12 cells) prepared by blade coating ((b) n-i-p PSC and (e) p-i-n PSC) and spin coating((c) n-i-p PSCs and (f) p-i-n PSC).

Declaration of Competing Interest

The authors declare that they have no known competing financial interests or personal relationships that could have appeared to influence the work reported in this paper.

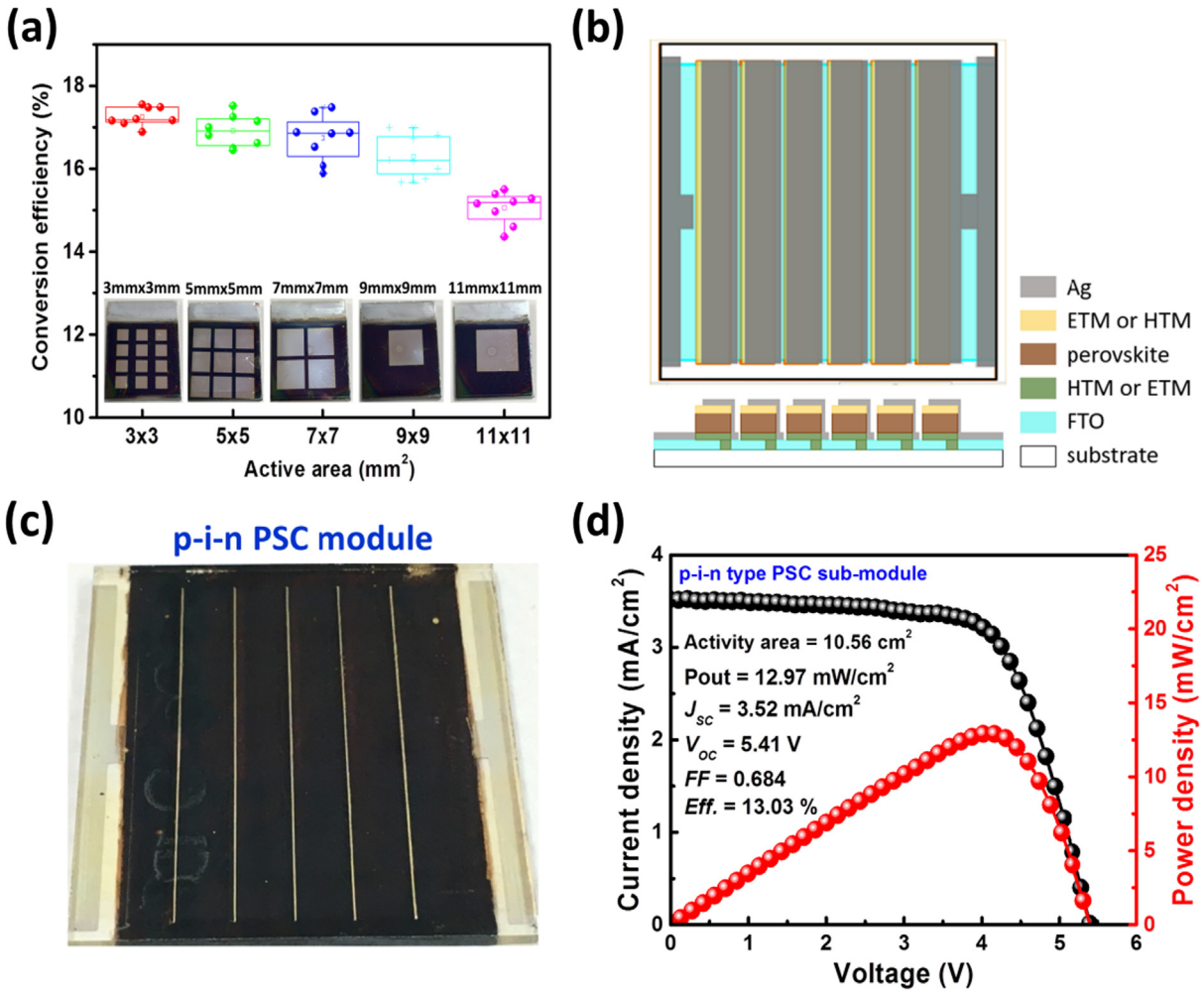

Fig. 10. (a) Statistical data of the conversion efficiency of PSCs with various active areas (inserted real device pictures). (b) Schematic of PSC sub-module architecture. (c) Picture of p-i-n PSC sub-module (5 cm × 5 cm), and (d) photovoltaic performance of p-i-n PSC sub-module by TABC process.

Acknowledgments

This work was supported by Ministry of Science and Technology, Taiwan (MOST 108-2628-E-182-003-MY3), Chang Gung University (QZRPD181) and Chang Gung Memorial Hospital, Linkou (CMRPD2J0041).

Appendix A. Supplementary material

Supplementary data to this article can be found online at https://doi.org/10.1016/j.solener.2020.05.003.

References

Barrows, A.T., Pearson, A.J., Kwak, C.K., Dunbar, A.D., Buckley, A.R., Lidzey, D.G., 2014. Efficient planar heterojunction mixed-halide perovskite solar cells deposited via spray-deposition. Energy Environ. Sci. 7 (9), 2944–2950.

Bi, Z., Rodríguez-Martínez, X., Aranda, C., Pascual-San-José, E., Goñi, A.R., Campoy-Quiles, M., et al., 2018. Defect tolerant perovskite solar cells from blade coated non-toxic solvents. J. Mater. Chem. A 6 (39), 19085–19093. https://doi.org/10.1039/c8ta06771f.

Chen, H., Wei, Z., Zheng, X., Yang, S., 2015. A scalable electrodeposition route to the low-cost, versatile and controllable fabrication of perovskite solar cells. Nano Energy 15, 216–226.

Cotella, G., Baker, J., Worsley, D., De Rossi, F., Pleydell-Pearce, C., Carnie, M., Watson, T., 2017. One-step deposition by slot-die coating of mixed lead halide perovskite for photovoltaic applications. Sol. Energy Mater. Sol. Cells 159, 362–369.

Das, S., Yang, B., Gu, G., Joshi, P.C., Ivanov, I.N., Rouleau, C.M., et al., 2015. High-performance flexible perovskite solar cells by using a combination of ultrasonic spray-coating and low thermal budget photonic curing. ACS Photonics 2 (6), 680–686.

Deng, Y., Dong, Q., Bi, C., Yuan, Y., Huang, J., 2016. Air-stable, efficient mixed-cation perovskite solar cells with Cu electrode by scalable fabrication of active layer. Adv. Energy Mater. 6 (11), 1600372. https://doi.org/10.1002/aenm.201600372.

Deng, Y., Peng, E., Shao, Y., Xiao, Z., Dong, Q., Huang, J., 2015a. Scalable fabrication of efficient organolead trihalide perovskite solar cells with doctor-bladed active layers. Energy Environ. Sci. 8 (5), 1544–1550.

Deng, Y., Wang, Q., Yuan, Y., Huang, J., 2015b. Vividly colorful hybrid perovskite solar cells by doctor-blade coating with perovskite photonic nanostructures. Mater. Horiz. 2 (6), 578–583.

Jung, M., Ji, S.-G., Kim, G., Seok, S.I., 2019. Perovskite precursor solution chemistry: from fundamentals to photovoltaic applications. Chem. Soc. Rev. 48 (7), 2011–2038. https://doi.org/10.1039/c8cs00656c.

Kim, J.H., Williams, S.T., Cho, N., Chueh, C.C., Jen, A.K.Y., 2015. Enhanced environmental stability of planar heterojunction perovskite solar cells based on blade-coating. Adv. Energy Mater. 5 (4), 1401229.

Kojima, A., Teshima, K., Shirai, Y., Miyasaka, T., 2009. Organometal halide perovskites as visible-light sensitizers for photovoltaic cells. J. Am. Chem. Soc. 131 (17), 6050–6051.

Laboratory, N.R.E., 2018. Best Research-Cell Efficiencies.

Lee, K.-M., Lin, C.-J., Liou, B.-Y., Yu, S.-M., Hsu, C.-C., Suryanarayanan, V., 2019. Effect of anti-solvent mixture on the performance of perovskite solar cells and suppression hysteresis behavior. Org. Electron. 65, 266–274. https://doi.org/10.1016/j.orgel.2018.08.048.

Leijtens, T., Eperon, G.E., Barker, A.J., Grancini, G., Zhang, W., Ball, J.M., et al., 2016. Carrier trapping and recombination: the role of defect physics in enhancing the open circuit voltage of metal halide perovskite solar cells. Energy Environ. Sci. 9 (11), 3472–3481. https://doi.org/10.1039/c6ee01729k.

Li, S.-G., Jiang, K.-J., Su, M.-J., Cui, X.-P., Huang, J.-H., Zhang, Q.-Q., et al., 2015. Inkjet printing of CH 3 NH 3 PbI 3 on a mesoscopic TiO 2 film for highly efficient perovskite solar cells. J. Mater. Chem. A 3 (17), 9092–9097.

Liang, K., Mitzi, D.B., Prikas, M.T., 1998. Synthesis and characterization of organic–inorganic perovskite thin films prepared using a versatile two-step dipping technique. Chem. Mater. 10 (1), 403–411.

Liu, Y., Liu, Z., Lee, E.-C., 2018. Dimethyl-sulfoxide-assisted improvement in the crystallization of lead-acetate-based perovskites for high-performance solar cells. J. Mater. Chem. C 6 (25), 6705–6713. https://doi.org/10.1039/c8tc01570h.

Paek, S., Schouwink, P., Athanasopoulou, E.N., Cho, K.T., Grancini, G., Lee, Y., et al., 2017. From nano- to micrometer scale: the role of antisolvent treatment on high performance perovskite solar cells. Chem. Mater. 29 (8), 3490–3498. https://doi.org/10.1021/acs.chemmater.6b05353.

Qin, T., Huang, W., Kim, J.-E., Vak, D., Forsyth, C., McNeill, C.R., Cheng, Y.-B., 2017. Amorphous hole-transporting layer in slot-die coated perovskite solar cells. Nano Energy 31, 210–217.

Razza, S., Di Giacomo, F., Matteocci, F., Cina, L., Palma, A.L., Casaluci, S., et al., 2015. Perovskite solar cells and large area modules (100 cm2) based on an air flow-assisted PbI2 blade coating deposition process. J. Power Sources 277, 286–291.

Tang, M.-C., Fan, Y., Barrit, D., Chang, X., Dang, H.X., Li, R., et al., 2020. Ambient blade coating of mixed cation, mixed halide perovskites without dripping: in situ investigation and highly efficient solar cells. J. Mater. Chem. A 8 (3), 1095–1104. https://doi.org/10.1039/c9ta12890e.

Tavakoli, M.M., Yadav, P., Prochowicz, D., Sponseller, M., Osherov, A., Bulović, V., Kong, J., 2019. Controllable perovskite crystallization via antisolvent technique using chloride additives for highly efficient planar perovskite solar cells. Adv. Energy Mater. 9 (17), 1803587. https://doi.org/10.1002/aenm.201803587.

Wei, Z., Chen, H., Yan, K., Yang, S., 2014. Inkjet printing and instant chemical transformation of a CH3NH3PbI3/nanocarbon electrode and interface for planar perovskite solar cells. Angew. Chem. Int. Ed. 53 (48), 13239–13243.

Wetzelaer, G.-J.A.H., Scheepers, M., Sempere, A.M., Momblona, C., Ávila, J., Bolink, H.J., 2015. Trap-assisted non-radiative recombination in organic-inorganic perovskite solar cells. Adv. Mater. 27 (11), 1837–1841. https://doi.org/10.1002/adma.201405372.

Whitaker, J.B., Kim, D.H., Larson, Bryon W., Zhang, F., Berry, J.J., van Hest, M.F.A.M., Zhu, K., 2018. Scalable slot-die coating of high performance perovskite solar cells. Sustain. Energy Fuels 2 (11), 2442–2449. https://doi.org/10.1039/c8se00368h.

Xie, L., Hwang, H., Kim, M., Kim, K., 2017. Ternary solvent for CH3NH3PbI3 perovskite films with uniform domain size. PCCP 19 (2), 1143–1150. https://doi.org/10.1039/c6cp06709c.

Xu, L., Che, S., Huang, J., Xie, D., Yao, Y., Wang, P., et al., 2019. Towards green anti-solvent for efficient CH3NH3PbBr 3 perovskite light emitting diodes: a comparison of toluene, chlorobenzene, and ethyl acetate. Appl. Phys. Lett. 115 (3), 033101. https://doi.org/10.1063/1.5094248.

Yang, M., Li, Z., Reese, M.O., Reid, O.G., Kim, D.H., Siol, S., et al., 2017. Perovskite ink with wide processing window for scalable high-efficiency solar cells. Nat. Energy 2 (5), 17038.

Yang, Z., Chueh, C.C., Zuo, F., Kim, J.H., Liang, P.W., Jen, A.K.Y., 2015. High-performance fully printable perovskite solar cells via blade-coating technique under the ambient condition. Adv. Energy Mater. 5 (13), 1500328.

Ye, F., Xie, F., Yin, M., He, J., Wang, Y., Tang, W., et al., 2017. Effect of thermal-convection-induced defects on the performance of perovskite solar cells. Appl. Phys Express 10 (7), 075502. https://doi.org/10.7567/apex.10.075502.